Salt Doping in PEO-Containing Block Copolymers: Counterion and Concentration Effects

Wen-Shiue Young and Thomas H. Epps, III*

Department of Chemical Engineering, University of Delaware, Newark, Delaware 19716

Received December 16, 2008; Revised Manuscript Received February 10, 2009

ABSTRACT: The phase behavior of lithium salt-doped poly(styrene-*b*-ethylene oxide) (PS−PEO) was studied as a function of salt concentration, lithium (Li) counterion (X), and annealing temperature. Three LiX salts were employed in this work: $LiClO_4$, $LiCF_3SO_3$, and $LiAsF_6$. Increasing the salt doping ratio ([EO]:[Li]) from 48:1 to 3:1 led to morphological changes from hexagonally packed cylinders to lamellar morphologies; however, comparison between the small-angle X-ray scattering (SAXS) and transmission electron microscopy (TEM) results shows that the location of these morphological changes are altered by the different counterions. We interpret our SAXS, TEM, and differential scanning calorimetry data using strong segregation theory to estimate an effective interaction parameter (χ_{eff}) for our salt-doped copolymers. This χ_{eff} varies linearly with salt concentration for a single PS-PEO:LiX material; however, the slope for each $\chi_{eff,PS-PEO:LiX}$ is influenced by the nature of the counterion. We rationalize these effects by examining the Lewis acidity of each anion.

Introduction

Electrochemical devices such as batteries and fuel cells are promising solutions for clean and sustainable energy sources. Electrolytes that facilitate ion transport between electrodes are key components in these devices, and polymeric materials are potentially useful in this capacity.[1] Polymer electrolyte membranes for lithium batteries require high ionic conductivities to decrease the internal potential losses and adequate mechanical strength to reduce dendrite formation and prevent short-circuiting between electrodes.[1−3] Poly(ethylene oxide) [PEO] has been one of the most studied solvating polymers for lithium batteries since its alkali ion conductive properties were reported in 1973.[4] The high concentration of electron pairs and polarizability of the ether groups in PEO make it one of the most promising polymer electrolytes for solid-state lithium batteries. The lithium ion transport between complexation sites is assisted by the segmental motions of the PEO backbone. This implies that low glass transition temperature (T_g) and low crystallinity PEO-based electrolytes are favored to achieve high ionic conductivities at room temperature; however, the mechanical strength of these molten PEO-like electrolytes is weak.[3,5−7] In order to increase mechanical strength in PEO-containing membranes, poly(styrene) [PS] was chosen as a complementary block to strengthen the diblock copolymer in our study. Several researchers have studied the phase behavior and applications of PS−PEO block copolymers. Cheng et al. investigated the PEO crystal orientation and growth kinetics under nanoconfinement using PS−PEO block copolymers in various nanoconfined geometries.[8−11] For this system, the lamellar thickness and PEO crystal orientation can be tuned by varying the crystallization temperature. In other work, Mao and Hillmyer used gyroid-forming PS−PEO thin films to create a PS template with three-dimensional nanochannels.[12] In both cases, the researchers take advantage of the mechanical strength of the PS domains.

To achieve high ionic conductivities, most salt-doping in PEO (and PEO-like) copolymers has focused on the low salt concentration regime, analogous to ether oxygen to lithium cation ([EO]:[Li]) ratios ranging from 50:1 to 6:1, and several studies have shown that salt doping can change the morphologies and thermal properties of block copolymers.[13−16] Ruzette et al. observed a significant increase in the order−disorder transition temperature (T_{ODT}) upon $LiCF_3SO_3$ doping in poly(methyl methacrylate-*b*-oligooxyethylene methacrylate) [PMMA−POEM].[17] Epps et al. investigated the phase behavior of $LiClO_4$-doped poly(styrene-*b*-isoprene-*b*-ethylene oxide) [PS−PI−PEO] and poly(isoprene-*b*-styrene-*b*-ethylene oxide) [PI−PS−PEO].[18,19] In these systems, increases in T_{ODT} and domain spacing, along with morphological changes, were found and attributed to an increase in the segmental interaction parameters (χ) as a function of salt concentration. Additionally, Lee et al. found that the domain spacing in poly(styrene-*b*-2-vinylpyridine) [PS−P2VP] and poly(styrene-*b*-4-vinylpyridine) [PS−P4VP] systems were strongly affected by the coordination type with cadmium chloride [$CdCl_2$], and only the PS−P2VP system exhibited a domain spacing increase upon the salt doping.[20] Kim et al. studied salt complexation effects in the PS−PEO system, and they found that the orientation and lateral ordering of microdomains were increased by the doping of a selective alkali halide salt.[21] Recently, Wang et al. reported ion complexation effects in the poly(styrene-*b*-methyl methacrylate) [PS−PMMA] system with lithium chloride [LiCl] and copper chloride [$CuCl_2$].[22] They also found an increase in microdomain spacing and ordering in PS−PMMA due to lithium−PMMA interactions. These morphology and thermal property changes affect the copolymer electrolytes' mechanical strength and ionic conductivity;[23] thus, studies of salt-doping effects on the block copolymer morphologies are necessary.

In this study, we report the effects of salt doping on the phase behavior of PS−PEO:LiX ($X = ClO_4^-$, $CF_3SO_3^-$, AsF_6^-) systems. Our work differs from previous studies in that we explore the effects of salt doping on the domain spacing, effective interaction parameter, and diblock copolymer morphology over a wide range of salt concentrations using several counterions. In particular, we demonstrate the relationships between effective interaction parameter and salt concentration and salt counterion. These relationships provide an understanding of the role that counterions play in PEO-containing block copolymer electrolyte assembly.

Experimental Section

Materials. PS−PEO was obtained from Polymer Source and had a molecular weight of 14 500 g/mol ($M_w/M_n = 1.05$) and a PS volume fraction of $f_{PS} = 0.68$ (calculated using homopolymer

* To whom correspondence should be addressed. E-mail: thepps@udel.edu.

10.1021/ma802799p CCC: $40.75
Published on Web 03/13/2009

densities at 140 °C).[24] Before transferring the PS−PEO into an argon-filled glovebox, the material was dried for 24 h under dynamic vacuum. Tetrahydrofuran (THF) was argon-purged and further dried by passage through two neutral alumina columns before use. Lithium perchlorate ($LiClO_4$), lithium trifluoromethanesulfonate ($LiCF_3SO_3$), and lithium hexafluoroarsenate ($LiAsF_6$) were obtained from Aldrich and used as received. All salts were stored in the glovebox. Because polymer electrolyte complexes, such as PEO:Li^+, are very hygroscopic, it is important to ensure that the experimental results are not affected by moisture uptake.[19,25,26] Therefore, we dried our block copolymer and solvent rigorously, and all further sample handling was performed in the glovebox.

Sample Preparation. The salt-doped PS−PEO samples were prepared in the glovebox. A measured amount of salt and PS−PEO was dissolved in THF, sealed in a drying chamber, and then dried under dynamic vacuum on a glass manifold. Following drying, samples were transferred back to the glovebox for storage.

Small-Angle X-ray Scattering (SAXS). SAXS experiments were performed in the Department of Chemical Engineering at the University of Delaware. A SAXS instrument, consisting of a three-pinhole collimation system with a 2 kW sealed-tube X-ray generator (Cu Kα, 1.54 Å), was used for our experiments. The sample-to-detector distance was 2000 mm. SAXS data were collected on a 2-dimensional multiwire detector. To study the effect of temperature on phase behavior, the SAXS chamber was equipped with a Linkam THMS600 stage. The SAXS sample cells were sealed in the glovebox, and the scattering experiments were conducted under vacuum at the desired temperature. All SAXS data are presented as the logarithmic scattering intensity vs the magnitude of the scattering vector, $|\mathbf{q}|$. All data are reported from cooling scans, where the samples were heated to 202 °C (unless otherwise noted) and annealed for 1 h prior to cooling. Samples were annealed at each acquisition temperature for 1 h, and the acquisition time was 1 h.

Transmission Electron Microscopy (TEM). TEM measurements were performed on a JEOL JEM-2000FX at an accelerating voltage of 200 kV. Samples were annealed in the SAXS chamber and then sectioned to ∼70 nm thickness at −60 °C using a Leica Reichart Ultracut S microtome with a cryo-attachment. The thin sections were collected onto 400 mesh TEM grids and stained using ruthenium tetraoxide (RuO_4) vapor at room temperature for ∼7 min to enhance contrast.

Differential Scanning Calorimetry (DSC). DSC experiments were conducted on a Perkin-Elmer Pyris Diamond DSC with a Cryofill liquid nitrogen attachment. A measured amount of sample between 4 and 8 mg was sealed in a 0219-0062 aluminum pan in the glovebox. Isobaric temperature ramps were conducted at a constant heating/cooling rate (10 °C/min). The DSC system was cooled to −100 °C and allowed to thermally equilibrate prior to performing temperature scans. All samples had a temperature scan range of −100 to 200 °C, except for the $LiAsF_6$-doped PS−PEO materials which had a scan range of −100 to 150 °C. Second heating scans are presented in this work.

Results

Neat and lithium-doped diblock copolymers were examined through a combination of SAXS, TEM, and DSC experiments. An in-situ SAXS profile for the neat PS−PEO sample at 28 °C exhibits a diffraction peak at 0.448 nm^{-1} (Figure 1). The inset to Figure 1 shows a TEM image of the neat PS−PEO sample, which was annealed at 166 °C for 12 h and then cooled to room temperature at 1 °C/min prior to sectioning on a cryo-ultramicrotome. The TEM image shows a hexagonally packed morphology, with a domain spacing of ∼13 nm. This value is reasonable when compared to the SAXS result (14.0 nm at 28 °C).

$LiClO_4$-Doped PS−PEO. Figure 2a shows in-situ SAXS profiles of PS−PEO:$LiClO_4$ as a function of salt-doping ratio ([EO]:[Li]) obtained at 166 °C. As the lithium salt concentration increases from 48:1 to 3:1, the primary scattering peak shifts

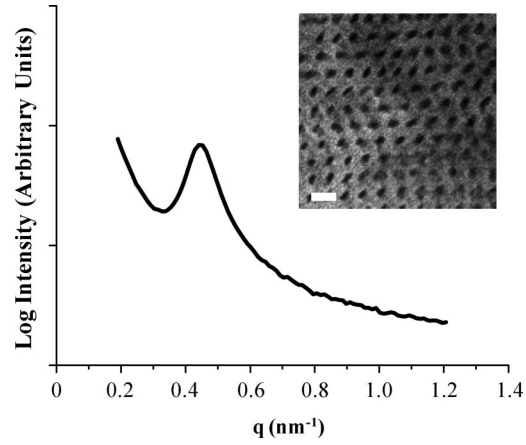

Figure 1. In-situ SAXS profile and TEM micrograph of PS−PEO neat sample at 28 °C. The TEM sample was annealed at 166 °C for 12 h and then slowly cooled down to room temperature. The scale bar in the TEM image represents 20 nm.

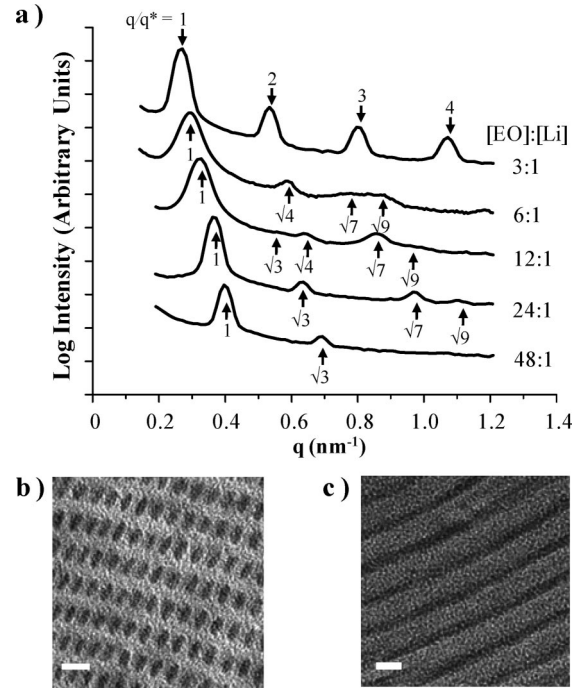

Figure 2. (a) In-situ SAXS profile of $LiClO_4$-doped PS−PEO vs salt concentration. The SAXS data were obtained at 166 °C. The diffraction peaks are identified by q/q^*, where q^* is the primary diffraction peak. Samples with salt-doping ratios from 48:1 to 6:1 exhibit a hexagonally packed morphology with Bragg reflection peaks located at q^*, $\sqrt{3}q^*$, $\sqrt{4}q^*$, $\sqrt{7}q^*$, and $\sqrt{9}q^*$. The 3:1 doping ratio sample exhibits a lamellar structure with Bragg reflection peaks located at q^*, $2q^*$, $3q^*$, and $4q^*$. Curves are shifted vertically for clarity. (b) TEM image of $LiClO_4$-doped PS−PEO 6:1 doping ratio sample. (c) TEM image of $LiClO_4$-doped PS−PEO 3:1 doping ratio sample. PEO domains were stained using RuO_4 vapor. The scale bars represent 20 nm.

to smaller q values (larger domain spacings). This shift is expected as salt doping has been previously shown to induce chain stretching.[18−21] The PS−PEO:$LiClO_4$ samples with doping ratios from 48:1 to 6:1 exhibit a hexagonally packed structure with Bragg reflection peaks located at q^*, $\sqrt{3}q^*$, $\sqrt{4}q^*$, $\sqrt{7}q^*$, and $\sqrt{9}q^*$, while the 3:1 material exhibits a lamellar structure with Bragg reflection peaks located at q^*, $2q^*$, $3q^*$, and $4q^*$. Thus, $LiClO_4$-doping in PS−PEO causes a cylinder to lamellae phase transition between the 6:1 and 3:1 $LiClO_4$ doping ratios. Figure 2b is the TEM image of the PS−PEO:$LiClO_4$ 6:1 sample which is consistent with a hexagonally

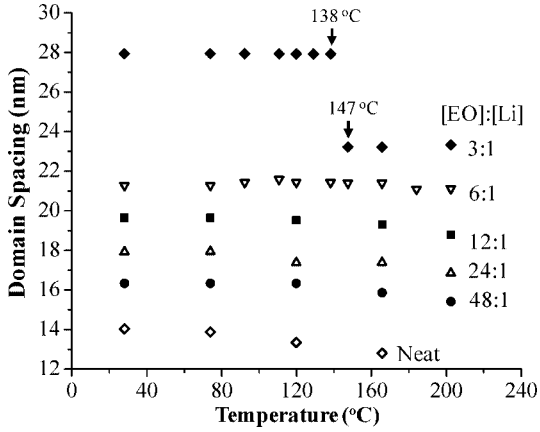

Figure 3. Domain spacing vs temperature calculated from in-situ SAXS cooling data for $LiClO_4$-doped PS−PEO samples at various salt-doping levels. Samples were held at temperature for 1 h prior to data acquisition, except for the 3:1 sample at 138 °C which was held at temperature for 9 h.

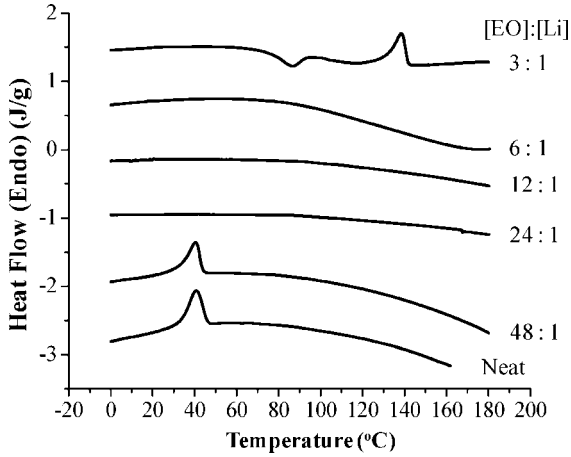

Figure 4. Second heating DSC ramps of $LiClO_4$-doped PS−PEO samples at various doping levels. The temperature scan range for all samples is -100 to 200 °C. The heating rate is 10 °C/min. Melting peaks of PEO are found in the neat and 48:1 samples. Crystallization and melting peaks of the PS−PEO:$LiClO_4$ 3:1 complex are shown in 3:1 sample. Curves are shifted vertically for clarity.

packed cylindrical morphology, and Figure 2c is the TEM image of the PS−PEO:$LiClO_4$ 3:1 sample which is consistent with a lamellar morphology. These images are in agreement with the symmetries (cylindrical and lamellar) determined from SAXS profiles. Additionally, there is good agreement between measured SAXS and TEM length scales.

Figure 3 summarizes the domain spacing data as a function of temperature and salt-doping ratio for PS−PEO:$LiClO_4$ obtained from the SAXS experiments (on cooling). The domain spacings increase as the salt concentration changes from neat (14.0 nm) to 3:1 (27.9 nm) at 28 °C. Additionally, for the neat, 48:1, 24:1, 12:1, and 6:1 specimens, the domain spacing displays a moderate inverse relationship to temperature. For the PS−PEO:$LiClO_4$ 3:1 sample, the domain spacing profile shows a discontinuity between 147 and 138 °C, where the domain spacing increases from 23.2 to 27.9 nm, upon cooling across this transition. The existence of a crystallization induced transition between two lamellar structures with different domain spacings to explain this behavior was presented in a previous work.[27]

DSC data for the PS−PEO:$LiClO_4$ materials are shown in Figure 4. For the neat sample, we locate an endothermic peak at 41 °C, which can be attributed to the melting of PEO

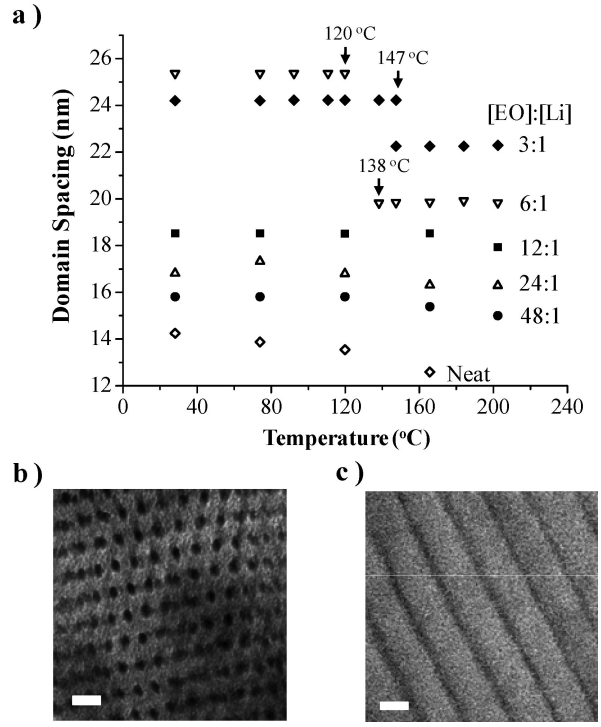

Figure 5. (a) Domain spacing vs temperature calculated from in-situ SAXS results for $LiCF_3SO_3$-doped PS−PEO samples at various salt-doping levels. (b) TEM image of $LiCF_3SO_3$-doped PS-PEO 24:1 sample. (c) TEM image of $LiCF_3SO_3$-doped PS-PEO 3:1 sample. The PEO domains were stained with RuO_4 vapor. The scale bars represent 20 nm.

crystallites. The degree of crystallinity was 35%, based on the enthalpy of formation for crystalline PEO of 213 J/g.[28] The PS−PEO:$LiClO_4$ 48:1 specimen also shows a PEO melting peak, and the degree of crystallinity is estimated to be 26%. No pure PEO melting peaks were found for doping ratios of 24:1 or higher, likely a result of the slow crystallization as we approach the eutectic point ([EO]:[Li] ∼ 10:1 for PEO:$LiClO_4$) and the reduction of chain mobility due to EO:Li coordination.[19,29] An endothermic peak is located at 139 °C for the PS−PEO:$LiClO_4$ 3:1 sample. Comparison of our results with the phase diagram of $LiClO_4$-doped PEO homopolymer indicates that this endotherm is likely due to the melting of a PS−PEO:$LiClO_4$ 3:1 complex. The melting point of the homopolymer PEO:$LiClO_4$ 3:1 complex given by Robitaille and Fauteux is 158 °C.[13] Using homopolymer/salt melting temperature data and also accounting for the maximum EO/Li crystallite size in the copolymer (estimated from the domain spacings in Figure 3) yields a calculated $T_{m,PEO/Li}$ of 135 °C (PS−PEO:$LiClO_4$ 3:1 complex), which is in reasonable agreement with the DSC data.[13,19,30] The DSC trace for the PS−PEO:$LiClO_4$ 3:1 sample also shows an exothermic crystallization peak at 87 °C.

$LiCF_3SO_3$-Doped PS−PEO. In-situ SAXS profiles of PS-PEO:$LiCF_3SO_3$ versus salt-doping level at 166 °C (Supporting Information) indicate that the PS−PEO:$LiCF_3SO_3$ phase behavior is similar to the PS−PEO:$LiClO_4$ behavior (Figure 2a), with a few minor differences. At low doping ratios (from 48:1 to 12:1), PS−PEO:$LiCF_3SO_3$ diffraction patterns are consistent with a hexagonally packed cylindrical morphology. For high doping ratios (6:1 and 3:1), PS−PEO:$LiCF_3SO_3$ samples display reflections indicative of a lamellar structure.

The temperature- and salt concentration-dependent domain spacing data for PS−PEO:$LiCF_3SO_3$ are shown in Figure 5a. The PS−PEO:$LiCF_3SO_3$ domain spacing data show a trend similar to the PS−PEO:$LiClO_4$ materials, except for the 6:1 doped material. From the in-situ SAXS profile of PS−PEO:

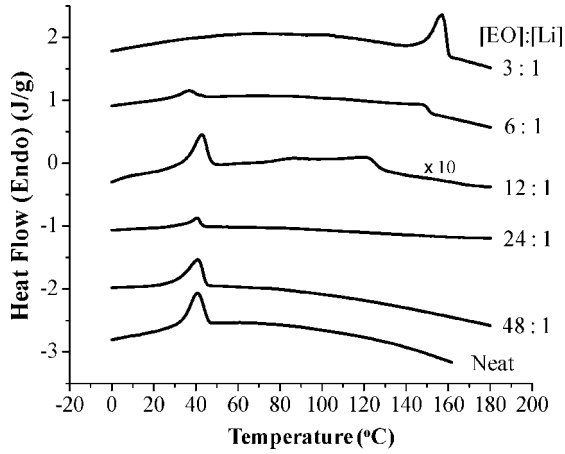

Figure 6. Second heating DSC ramps of $LiCF_3SO_3$-doped PS−PEO samples at various doping levels. The temperature scan range for all samples is -100 to 200 °C. The heating rate is 10 °C/min. Pure PEO melting peaks are found in all samples, except in the 3:1 specimen. Melting peaks for PS−PEO:$LiCF_3SO_3$ 3:1 complex are shown in the 12:1, 6:1, and 3:1 samples. The intensity of 12:1 sample is multiplied by a factor of 10. Curves are shifted vertically for clarity.

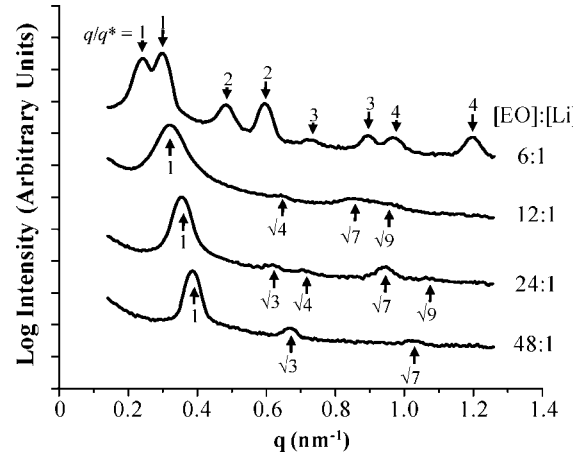

Figure 7. In-situ SAXS profiles of $LiAsF_6$-doped PS−PEO samples at 120 °C. The diffraction peaks of the 48:1, 24:1, and 12:1 samples are consistent with hexagonally packed structure. The 6:1 sample exhibits two sets of diffraction peaks which are consistent with phase coexistence of two lamellar structures (short arrow [low temperature] set and long arrow [high temperature] set). Curves are shifted vertically for clarity.

$LiCF_3SO_3$ 6:1 sample (Supporting Information), at temperatures below 120 °C, we observe peak growth at smaller q (larger domain spacing), but the q^* peak that exists at temperatures higher than 120 °C does not disappear. This implies that there is phase coexistence at temperatures below 120 °C. Comparison to the $LiCF_3SO_3$-doped PEO homopolymer phase diagram indicates that the two phases are a low concentration PEO−$LiCF_3SO_3$ solution and a PEO:$LiCF_3SO_3$ 3:1 complex.[13] The TEM image of PS−PEO:$LiCF_3SO_3$ 24:1 (Figure 5b) indicates that the 24:1 sample has a hexagonally packed cylindrical morphology, and the TEM image of PS−PEO:$LiCF_3SO_3$ 3:1 (Figure 5c) shows that the 3:1 sample has a lamellar morphology. These micrographs are consistent with the symmetries (cylindrical and lamellar) determined from SAXS profiles. Again, there is good agreement between the domain spacings, d^*, determined by SAXS and TEM.

In Figure 6, we show the DSC traces of the PS−PEO:$LiCF_3SO_3$ system. As the doping level increases from the neat sample to the 6:1 specimen, the PEO melting peak area decreases (note: the 12:1 curve is enlarged by a factor of 10). Additionally, the 12:1 sample exhibits a small PEO:$LiCF_3SO_3$ complex melting peak at 122 °C. The 6:1 trace shows a PEO:$LiCF_3SO_3$ complex melting peak at 148 °C, in addition to the small PEO melting peak, which is evidence of the phase separation in the PS−PEO:$LiCF_3SO_3$ 6:1 material. An endothermic peak is located at 157 °C for the PS−PEO:$LiCF_3SO_3$ 3:1 sample. Comparison of our results with the phase diagram of $LiCF_3SO_3$-doped PEO homopolymer indicates that this endotherm is likely due to the melting of the PEO:$LiCF_3SO_3$ 3:1 complex.

$LiAsF_6$-Doped PS−PEO. Figure 7 displays the SAXS profiles of PS−PEO:$LiAsF_6$ samples at 120 °C. In this system, the samples are not thermally stable at 166 °C; thus, we set the highest SAXS annealing temperature to 138 °C to obtain the reversible results from the X-ray scattering. At low doping levels, from 48:1 to 12:1, $LiAsF_6$-doped PS−PEO samples exhibit a hexagonally packed cylindrical structure. A change in morphology occurs between the 12:1 and 6:1 doping levels, as the 6:1 doping ratio sample exhibits two distinct sets of diffraction peaks, both of which can be assigned according to lamellar symmetry (short arrow [low temperature] set and long arrow [high temperature] set on the 6:1 line; see Supporting Information for the thermal SAXS data for the PS−PEO:$LiAsF_6$ 6:1 specimen). Because the PEO:$LiAsF_6$ 6:1 complex has a

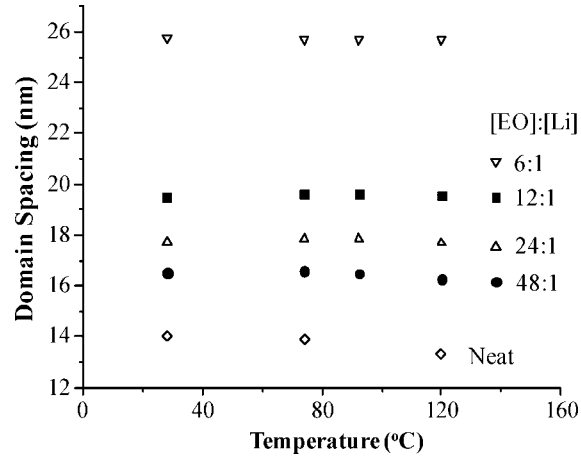

Figure 8. Domain spacing vs temperature calculated from in-situ SAXS results for $LiAsF_6$-doped PS−PEO samples at various doping levels. The annealing time at each temperature is 1 h for all samples. Note that the 6:1 sample exhibits two sets of diffraction peaks at temperatures below 120 °C, and the data points in this figure are calculated from the smaller q^* data.

melting point around 120 °C (to be discussed in the DSC result), a portion of the sample crystallizes and forms a larger domain spacing lamellar structure, while the remaining amorphous material accounts for the smaller domain spacing lamellar structure in the cooling data at 120 °C. This phase behavior is similar to the PS−PEO:$LiClO_4$ 3:1 sample and PS−PEO:$LiCF_3SO_3$ 3:1 sample as discussed in our previous work.[27] The PS−PEO:$LiAsF_6$ 3:1 doping ratio sample is not included in this figure because the specimen's thermal instability at elevated temperatures (as noted by visual inspection and the lack of reversibility on subsequent heating and cooling SAXS scans) prevented us from following a similar annealing protocol to the other samples.

The PS−PEO:$LiAsF_6$ domain spacing data for all doping levels and temperatures are shown in Figure 8. Data were obtained from the in-situ SAXS profiles. The 48:1, 24:1, and 12:1 samples show a trend similar to the PS−PEO:$LiClO_4$ and PS−PEO:$LiCF_3SO_3$ materials. The 6:1 doping level sample shows a domain spacing discontinuity at 120 °C due to crystallization of the 6:1 PEO−$LiAsF_6$ complex.

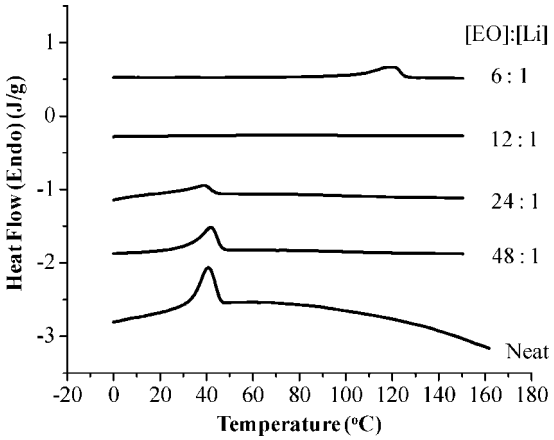

Figure 9. Second heating DSC ramps of $LiAsF_6$-doped PS−PEO samples at various doping levels. The temperature scan range for all samples is -100 to 150 °C. The heating rate is 10 °C/min. Pure PEO melting peaks are found in the neat, 48:1, and 24:1 samples. A melting peak for the PS−PEO:$LiAsF_6$ 6:1 complex is located at 120 °C. Curves are shifted vertically for clarity.

Figure 9 shows the DSC traces for the $LiAsF_6$-doped PS−PEO samples. At the low salt concentrations (48:1 and 24:1), a PEO melting peak was located, where the crystallinity of the PEO domain decreases as the salt concentration increases. At high salt concentrations, the PEO melting peak has disappeared. Instead, a higher temperature melting peak corresponding to the PEO:salt complex is found at 120 °C for the 6:1 specimen. The 120 °C melting peak in the 6:1 PS−PEO:$LiAsF_6$ material is consistent with the phase transition shown in our SAXS data.

The domain spacing data for each of our three lithium salt-doped materials are summarized in Figure 10. Figure 10a shows the domain spacing vs salt concentration data at 166 °C. Because the PS−PEO:$LiAsF_6$ samples are not thermally stable at 166 °C, we compare only the $LiClO_4$-doped PS−PEO and $LiCF_3SO_3$-doped PS−PEO systems at this temperature. As the salt concentration increases, the domain spacings of both $LiClO_4$-doped and $LiCF_3SO_3$-doped PS−PEO increase. At all doping levels the domain spacings of the $LiClO_4$-doped system are higher than those of the $LiCF_3SO_3$-doped system. Figure 10b shows the domain spacing vs salt concentration data of salt-doped PS−PEO systems at 120 °C. For low salt concentrations from 48:1 to 12:1, the $LiAsF_6$-doped system has the highest domain spacing while the $LiCF_3SO_3$-doped system has the lowest domain spacing. At the 6:1 doping ratio, both the $LiCF_3SO_3$-doped and $LiAsF_6$-doped samples show larger domain spacings than the $LiClO_4$-doped material. This anomaly occurs as a result of PEO−salt complex crystallization in the 6:1 $LiCF_3SO_3$ and $LiAsF_6$-doped samples, but not the 6:1 $LiClO_4$-doped specimen, as described earlier in the text.

Discussion

The domain spacing behavior of the PS−PEO block copolymers doped with three lithium salts is summarized in Figure 10. In all cases, we find that increasing the salt concentration leads to larger domain spacings. Although the increase of domain spacing upon salt-doping may be partially attributed to the volume of salt added to the copolymer, this effect alone does not account for the full change in domain spacing. For example, the addition of $LiClO_4$ to PS−PEO would only lead to an increase the domain spacing from 12.8 to 14.3 nm for the PS−PEO:$LiClO_4$ 3:1 sample at 166 °C (assuming ideal mixing), which is much smaller than change noted from the X-ray scattering data (23.2 nm). This additional increase likely results from the interactions between the ether oxygens in the PEO

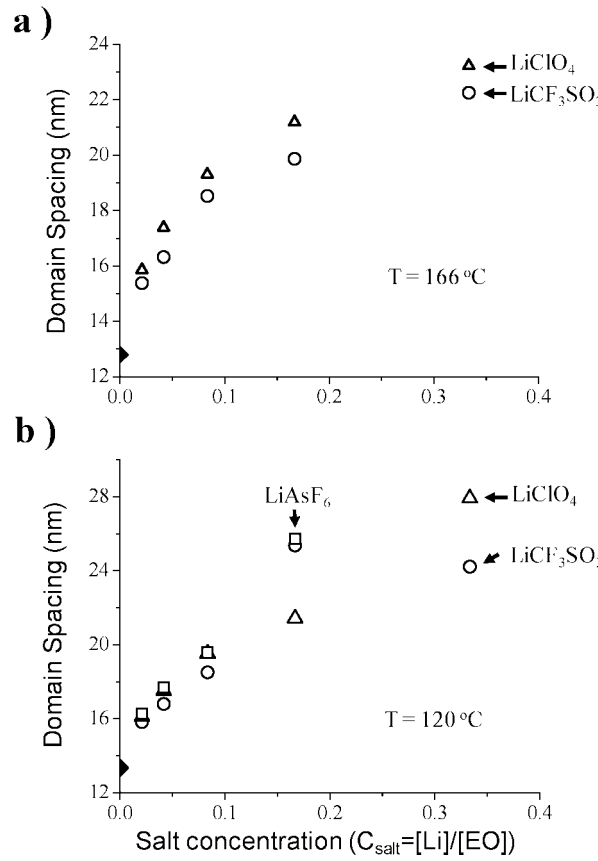

Figure 10. Domain spacing versus salt concentration ([Li]/[EO]) calculated from in-situ SAXS data at (a) 166 °C and (b) 120 °C. At 166 °C, the domain spacings of $LiClO_4$-doped PS−PEO samples are higher than those of $LiCF_3SO_3$-doped PS−PEO specimens at all doping levels. At 120 °C, the domain spacings of $LiAsF_6$-doped samples are the largest among these three salt-doped systems at doping levels of 48:1, 24:1, and 12:1.

backbone and the Li cations, where the coordination complexes for each of the PEO/lithium salt ratios described in this work can be found in the literature.[13] Furthermore, the discontinuity in domain spacing vs temperature for the PS−PEO:$LiClO_4$ (3:1) and PS−PEO:$LiCF_3SO_3$ (6:1 and 3:1) systems has been explained in previous work.[27] For the PS−PEO:$LiClO_4$ 3:1 material, the domain spacing, increases from 23.2 to 27.9 nm upon cooling the sample from 147 to 138 °C. X-ray scattering, along with TEM and DSC, confirmed the existence of a crystallization induced order−order transition in confined PEO domains. Similar behavior is found in the PS−PEO:$LiAsF_6$ system at the 6:1 doping level, as described in the Results section, and this explains the coexistence of the two lamellar structures shown in Figure 7.

Through detailed comparison between the thermal behavior of our salt-doped block copolymers (as determined by DSC) and the PEO homopolymer-doped behavior reported by Robitaille and Fauteux, we can conclude that the behavior in our system mimics that exhibited by their homopolymer materials once the nanostructure confinement effects are taken into account.[13] On the basis of literature data for $LiClO_4$-doped block copolymers, we can develop a relationship between melting temperature and inverse domain spacing.[19] Using this information, we can estimate the expected changes in melting temperature when the PEO samples examined by Robitaille et al. are confined in nanoscale domains. We calculate the slope of the melting temperature vs inverse PEO domain size ($1/w$) curve from the PEO melting temperature in Robitaille's work (where $1/w$ is approximately zero), the PEO melting temperature of

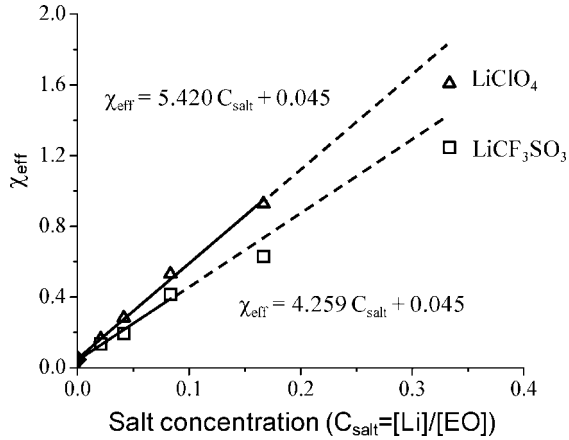

Figure 11. χ_{eff} vs salt concentration ([Li]/[EO]) at 166 °C. The χ of neat sample is obtained from literature. The χ_{eff} values for salt-doped samples are calculated using domain spacing data obtained from in-situ SAXS experiments and the relationship between domain spacing and χ in strong segregation regime. The linear regression lines (solid lines) were fit using only the cylinder-forming samples in each system, and the lines were force fit through χ of the neat sample. The regression lines, based on the cylinder-forming data, are extended to the lamellae-forming samples (dash lines).

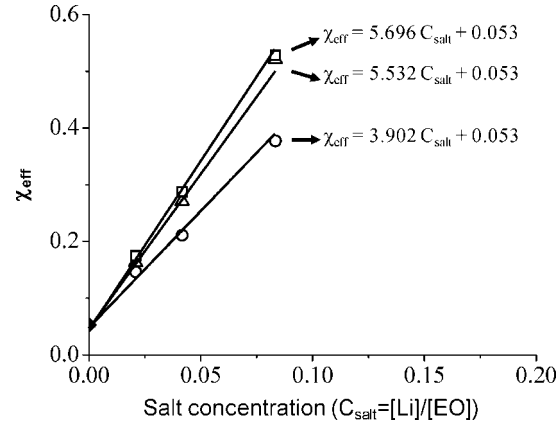

Figure 12. χ_{eff} vs salt concentration ([Li]/[EO]) at 120 °C. The low salt concentration samples show that χ_{eff} for each salt-doped system has a linear relationship with salt concentration, and the slope decreases from PS−PEO:$LiAsF_6$ (square) > PS−PEO:$LiClO_4$ (triangle) > PS−PEO:$LiCF_3SO_3$ (circle).

our neat sample (where $1/w$ is 0.136 nm^{-1}), and the data from Epps et al.[19] Using this slope, we determine the expected melting temperature of PEO:$LiClO_4$ 3:1 complex for our system ($1/w \sim 0.111$ nm^{-1}) to be 135 °C. Similarly, we obtain estimated melting temperatures for the PS−PEO:$LiCF_3SO_3$ 3:1 complex and PS−PEO:$LiAsF_6$ 6:1 complex of 158 and 111 °C, respectively. Thus, it is reasonable to assume that the structures reported in the literature are identical to the structures in our system, as actual data give 157 °C (see Figure 6 for PS−PEO:$LiCF_3SO_3$) and 120 °C (see Figure 9 for PS−PEO:$LiAsF_6$). Furthermore, the synergies between the homopolymer (PEO) and the block copolymer (PS−PEO)-doped phase diagrams strongly imply that nearly all of the lithium salt preferentially associates with the PEO domains in the block copolymer with no macroscopic phase separation. Data illustrating the behavior of polymer/salt complexes at the salt doping levels greater than 3:1 are not shown, as macroscopic phase separation of the lithium salt from the PEO occurs at these higher doping levels, as also noted in the homopolymer report.

By compiling the domain spacing data for each of the three PS−PEO:LiX complexes (where X = ClO_4, CF_3SO_3, AsF_6), we can estimate effective interaction parameters as a function of salt doping level and counterion composition. These effective interaction parameters, χ_{eff}, are calculated for each salt-doped sample relative to the interaction parameter of the neat sample, χ_{SO},[31] and the domain spacings obtained from the SAXS data. The relationship between domain spacings and effective interaction parameters of salt-doped PS−PEO samples are estimated using strong segregation behavior for diblock copolymers, $d^* \sim \chi^{1/6}$.[32,33] We note that the segregation strength of the neat sample ($\chi N \sim 18$ at 28 °C) is in the intermediate regime instead of the strong segregation regime ($\chi N > 100$); however, the exponential dependence of d^* vs χ varies from ~1/5 to 1/6 in this range.[34] While this may cause a slight overestimation of the χ_{eff} values, our results still show a reasonable relationship between salt doping concentration and χ_{eff}. The results of these calculations are shown in Figures 11 and 12. In Figure 11, the χ_{eff} data estimated using the neat sample χ and domain spacings of salt-doped samples at 166 °C show a linear relationship with salt concentration ([Li]/[EO]) for both the $LiClO_4$-doped and $LiCF_3SO_3$-doped systems. (The PS−PEO:$LiAsF_6$ samples are not thermally stable at 166 °C and thus are not included in this figure.) From the DSC results, we know that both the PS and PEO:salt domains are in the molten state at 166 °C. We note that only cylinder-forming samples are used to fit the regression lines (solid lines) due to a possible prefactor difference between the cylindrical and lamellar morphologies. The regression lines are extended to the lamellae-forming samples (dash lines) where we find that the calculated χ_{eff} values are ~15% lower than the extensions of the regression lines, though the overall trend is preserved. We also have not explicitly accounted for changes in statistical segment length upon salt addition in the above calculation; however, we note that Wang et al. found a ~10% increase in segmental length when adding lithium salt in PS−PMMA copolymers (from neat sample to highest doping level sample).[35] We would expect some deviation in this behavior for our system due to differences between Li:PEO and Li:PMMA interactions.

That we can fit our domain spacing data in Figure 11 using only a change in χ_{eff} possibly indicates that the number of effective repeat units is not changed by salt doping;[36] however, further experiments are needed to support this assertion. The $LiClO_4$-doped system has a higher slope due to its larger domain spacing at each salt doping level. We hypothesize that because the ClO_4^- is the weaker Lewis base (meaning ClO_4^- has weaker interaction with Li^+), Li^+ has a stronger association with the PEO chains leading to increased PEO chain stretching to accommodate the lithium ions.[37] Therefore, the addition of $LiClO_4$ increases the effective interaction parameter, χ_{eff}, more than $LiCF_3SO_3$. In Figure 12, we show the effective interaciton parameter vs salt concentration data for the salt-doped PS−PEO systems at 120 °C. At low doping ratios from 48:1 to 12:1, the $LiAsF_6$-doped curve displays the largest slope while the $LiCF_3SO_3$-doped curve shows the smallest slope. This matches with our above hypothesis, as AsF_6^- is the weakest Lewis base and $CF_3SO_3^-$ is the strongest Lewis base of our three counterions. At the highest doping ratios (6:1 and 3:1), the effective interaction parameters of these three salt-doped systems no longer show linear relationships with salt concentration at 120 °C due to crystallization of the PEO−salt complexes. Thus, in the absence of crystallization effects, the addition of $LiAsF_6$ leads to the largest increase in our χ_{eff} parameter. Overall, the addition of the lithium salts increases the $\chi_{eff}N$ values from ~10.5 (neat material) to ~ 377 (PS−PEO:$LiClO_4$ 3:1 material) at 166 °C, showing that salt doping provides an efficient method for manipulating interactions over a wide range.

Conclusion

Using TEM, DSC, and temperature-controlled SAXS, we evaluate the effects of lithium salt counterions on the phase

behavior of doped PS−PEO diblock copolymers. Salt doping leads to an increase in segregation strength for all PS−PEO:LiX ($X = ClO_4^-$, $CF_3SO_3^-$, AsF_6^-) systems as illustrated by increases in domain spacings. Additionally, increasing the salt concentrations from 48:1 to 3:1 ([EO]:[Li]) leads to morphological changes from hexagonally packed cylinders to lamellar morphologies.

We also examine the thermal behavior of these three PS−PEO/salt systems. Through DSC analysis, we find that the phase behavior of the comparable salt-doped PEO domains is consistent with binary phase diagrams for the salt-doped PEO homopolymers. This implies that all of the lithium salt resides in the PEO domains at doping ratios up to 3:1. Furthermore, crystallization of the PEO salt complexes above the glass transition temperature of the poly(styrene) block leads to discontinuous changes in domain spacing as a function of temperature. As further evidence of the increase in segregation strength upon doping, these crystallization-induced transitions are confined within the previously established lamellar domains.

Finally, we find a linear relationship between χ_{eff} and salt concentration in each of our salt-doped PS−PEO systems, where χ_{eff} is estimated from the strong segregation theory. By comparing the three lithium salts, we note that $LiAsF_6$-doping shows the largest increase in segregation strength at a given salt concentration, which we relate to the weaker Lewis base character of the AsF_6^- relative to the other two lithium counterions. This difference in counterion activity leads to differences in the domain spacing (and segregation strength) between the various copolymer:salt complexes and ultimately differences in their phase behavior at similar lithium ion concentrations.

Acknowledgment. This work was supported by the ACS through Grant PRF-46864-67. We thank the Delaware Biotechnology Institute (DBI) for assistance in purchasing the Rigaku small-angle X-ray scattering instrument. TEM was performed at W.M. Keck Microscopy Facility at the University of Delaware. We also thank Ghulam Hassnain Jaffari, Dr. Xinqiao Jia, and Dr. John Rabolt for permitting usage of their calorimetry facilities.

Supporting Information Available: In-situ SAXS profiles of PS−PEO:$LiCF_3SO_3$ vs salt-doping level at 166 °C, in-situ SAXS profiles of PS−PEO:$LiCF_3SO_3$ 6:1 vs temperature, and in-situ SAXS profiles of PS−PEO:$LiAsF_6$ 6:1 vs temperature. This material is available free of charge via the Internet at http://pubs.acs.org.

References and Notes

(1) Ratner, M. A.; Shriver, D. F. *Chem. Rev.* **1988**, *88* (1), 109–124.
(2) Abouimrane, A.; Alarco, P.-J.; Abu-Lebdeh, Y.; Davidson, I.; Armand, M. *J. Power Sources* **2007**, *174* (2), 1193–1196.
(3) Tarascon, J. M.; Armand, M. *Nature (London)* **2001**, *414* (6861), 359–367.
(4) Meyer, H. W. *Adv. Mater.* **1998**, *10* (6), 439–448.
(5) Lascaud, S.; Perrier, M.; Vallee, A.; Besner, S.; Prud'homme, J.; Armand, M. *Macromolecules* **1994**, *27* (25), 7469–7477.
(6) Minier, M.; Berthier, C.; Gorecki, W. *J. Phys. (Paris)* **1984**, *45*, 739–744 .
(7) Shi, J.; Vincent, C. A. *Solid State Ionics* **1993**, *60* (1−3), 11–17.
(8) Hsiao, M.-S.; Zheng, J. X.; Leng, S.; Van Horn, R. M.; Quirk, R. P.; Thomas, E. L.; Chen, H.-L.; Hsiao, B. S.; Rong, L.; Lotz, B.; Cheng, S. Z. D. *Macromolecules* **2008**, *41* (21), 8114–8123.
(9) Huang, P.; Zhu, L.; Guo, Y.; Ge, Q.; Jing, A. J.; Chen, W. Y.; Quirk, R. P.; Cheng, S. Z. D.; Thomas, E. L.; Lotz, B.; Hsiao, B. S.; Avila-Orta, C. A.; Sics, I. *Macromolecules* **2004**, *37* (10), 3689–3698.
(10) Sun, L.; Zhu, L.; Ge, Q.; Quirk, R. P.; Xue, C.; Cheng, S. Z. D.; Hsiao, B. S.; Avila-Orta, C. A.; Sics, I.; Cantino, M. E. *Polymer* **2004**, *45* (9), 2931–2939.
(11) Zhu, L.; Cheng, S. Z. D.; Calhoun, B. H.; Ge, Q.; Quirk, R. P.; Thomas, E. L.; Hsiao, B. S.; Yeh, F.; Lotz, B. *Polymer* **2001**, *42* (13), 5829–5839.
(12) Mao, H.; Hillmyer, M. A. *Soft Matter* **2006**, *2* (1), 57–59.
(13) Robitaille, C. D.; Fauteux, D. *J. Electrochem. Soc.* **1986**, *133* (2), 315–325.
(14) Staunton, E.; Andreev, Y. G.; Bruce, P. G. *Faraday Discuss.* **2007**, *134*, 143–156.
(15) Chandrasekhar, V. *Adv. Polym. Sci.* **1998**, *135*, 139–205.
(16) Fauteux, D.; McCabe, P. *Polym. Adv. Technol.* **1995**, *6* (2), 83–90.
(17) Ruzette, A.-V. G.; Soo, P. P.; Sadoway, D. R.; Mayes, A. M. *J. Electrochem. Soc.* **2001**, *148* (6), A537−A543.
(18) Epps, T. H.; Bailey, T. S.; Pham, H. D.; Bates, F. S. *Chem. Mater.* **2002**, *14* (4), 1706–1714.
(19) Epps, T. H.; Bailey, T. S.; Waletzko, R.; Bates, F. S. *Macromolecules* **2003**, *36* (8), 2873–2881.
(20) Lee, D. H.; Kim, H. Y.; Kim, J. K.; Huh, J.; Ryu, D. Y. *Macromolecules* **2006**, *39* (6), 2027–2030.
(21) Kim, S. H.; Misner, M. J.; Yang, L.; Gang, O.; Ocko, B. M.; Russell, T. P. *Macromolecules* **2006**, *39* (24), 8473–8479.
(22) Wang, J. Y.; Chen, W.; Roy, C.; Sievert, J. D.; Russell, T. P. *Macromolecules* **2008**, *41* (3), 963–969.
(23) Khandpur, A. K.; Foerster, S.; Bates, F. S.; Hamley, I. W.; Ryan, A. J.; Bras, W.; Almdal, K.; Mortensen, K. *Macromolecules* **1995**, *28* (26), 8796–8806.
(24) Fetters, L. J.; Lohse, D. J.; Richter, D.; Witten, T. A.; Zirkel, A. *Macromolecules* **1994**, *27* (17), 4639–4647.
(25) Bang, J.; Kim, B. J.; Stein, G. E.; Russell, T. P.; Li, X.; Wang, J.; Kramer, E. J.; Hawker, C. J. *Macromolecules* **2007**, *40* (19), 7019–7025.
(26) Singh, M.; Odusanya, O.; Wilmes, G. M.; Eitouni, H. B.; Gomez, E. D.; Patel, A. J.; Chen, V. L.; Park, M. J.; Fragouli, P.; Iatrou, H.; Hadjichristidis, N.; Cookson, D.; Balsara, N. P. *Macromolecules* **2007**, *40* (13), 4578–4585.
(27) Young, W.-S.; Brigandi, P. J.; Epps, T. H. *Macromolecules* **2008**, *41* (17), 6276–6279.
(28) Wieczorek, W.; Raducha, D.; Zalewska, A.; Stevens, J. R. *J. Phys. Chem. B* **1998**, *102* (44), 8725–8731.
(29) Watanabe, M.; Naganoa, S.; Sanuia, K.; Ogata, N. *Solid State Ionics* **1986**, *18−19* (1), 338–342.
(30) Weimann, P. A.; Hajduk, D. A.; Chu, C.; Chaffin, K. A.; Brodil, J. C.; Bates, F. S. *J. Polym. Sci., Part B: Polym. Phys.* **1999**, *37* (16), 2053–2068.
(31) Cochran, E. W.; Morse, D. C.; Bates, F. S. *Macromolecules* **2003**, *36* (3), 782–792.
(32) Lipic, P. M.; Bates, F. S.; Matsen, M. W. *J. Polym. Sci., Part B: Polym. Phys.* **1999**, *37* (16), 2229–2238.
(33) Semenov, A. N. *Macromolecules* **1989**, *22* (6), 2849–2851.
(34) Whitmore, M. D.; Vavasour, J. D. *Acta Polym.* **1995**, *46* (5), 341–360.
(35) Wang, J.-Y.; Chen, W.; Russell, T. P. *Macromolecules* **2008**, *41* (13), 4904–4907.
(36) Epps, T. H.; Bates, F. S. *Macromolecules* **2006**, *39* (7), 2676–2682.
(37) Andrew, W. *J. Electrochem. Soc.* **1991**, *138* (9), 2586–2590.

MA802799P